Non-equilibrium molecular dynamics simulations of the transient Ludwig-Soret effect in a binary Lennard-Jones/spline mixture

Bjørn Hafskjold

Department of Chemistry, Norwegian University of Science and Technology, N-7491 Trondheim, Norway

Email: bjorn.hafskjold@ntnu.no

Summary

A binary isotope mixture of Lennard-Jones/spline particles at equilibrium was perturbed by a sudden change in the system's boundary temperatures. The system's response was determined by non-equilibrium molecular dynamics (NEMD). Three transient processes were studied: (1) The propagation of a pressure (shock) wave, (2) heat diffusivity and conduction, and (3) thermal diffusion (the Ludwig-Soret effect). These three processes occur at different time scales, which makes it possible to separate them in one single NEMD run. The system was studied in liquid, supercritical, and dense gas states with various forms and strengths of the thermal perturbation. The results show that heat was initially transported by two separate mechanisms; (1) heat diffusion as described by the transient heat equation and (2) as a consequence of a pressure wave. The pressure wave travelled faster than the speed of sound, generating a shock wave in the system. Local equilibrium was found in the transient phase, even with very strong perturbations and in the shock front. Although the mass separation due to the Ludwig-Soret effect developed much slower than the pressure and temperature fields in the system at large, it was found that the Soret coefficient could be accurately determined from the initial phase of the transient and close to the heat source. This opens the possibility of a new way to analyse results from transient experiments and thereby minimize effects of gravity and convection due to buoyancy.

1. Introduction

The components of a fluid mixture in a temperature gradient will to a certain extent separate due to the Ludwig-Soret effect [1,2]. A measure of the effect is the ratio between the concentration gradient and the temperature gradient at stationary state, which can be quantified as the thermal diffusion factor or the Soret coefficient [3]. The Soret effect is one of the coupled transport processes in mixtures [3,4].

The Soret effect has been studied for many years, both experimentally and by computer simulations. High-quality data for binary and ternary mixtures are now available, see *e.g*. Bou-Ali [5] and references therein, and so are models with reasonable predictive power based on differences in molecular parameters such as mass, interaction energy, and molecular size [6-9]. However, the relationship between the molecular properties and the observed effect is still not developed to the extent that a robust, predictive model for the Soret coefficient is established.

A nice and recent review of experimental methods to determine Soret coefficients in binary and ternary mixtures was given by Köhler and Morozow [10]. Other excellent reviews were written by Srinivasan and Saghir [11], Platten [12], and Wiegand [13]. The methods that are of most interest in the context of the present paper are fast methods that work at very small length scale, such as optical beam deflection [14], thermal diffusion forced Rayleigh scattering [15,16], and optical digital interferometry [17].

Whereas a stationary-state thermal gradient is relatively quickly established in a fluid mixture, it takes longer to establish a stationary concentration gradient. A key dimensionless number is the ratio between the thermal and mass diffusivities, the Lewis number, which in a typical liquid mixture is of the order 100. Use of stationary-state methods is therefore often limited by the time it takes to reach a stable concentration gradient in the system. In order to avoid the effect of buoyancy and convection, which may corrupt the measurements of the Soret effect, different methods have been used [10], notably (1) Heating from the top of the sample, (2) zero-gravity measurements in ballistic flights or at

the International Space Station, and (3) transient methods. Fast transient methods have the advantage that they are not much affected by gravity and can therefore be used on Earth. A disadvantage is that the results are more difficult to interpret as compared with stationary-state methods.

Computer simulations represent another important tool in studies of the Soret effect. Equilibrium as well as non-equilibrium molecular dynamics (NEMD) have been used; a recent review was given by Artola and Rousseau [6]. In the last twenty years or so, synthetic [18, 19] and boundary-driven NEMD (BD-NEMD) [20-22] methods have gained interest because they appear to be quite suitable for the coupled transport processes such as the Soret effect. [23]

The work discussed in this paper is based on BD-NEMD. Several implementations of BD-NEMD methods are available, see *e.g*. Artola and Rousseau [6]. A common feature when applied to thermal or mass diffusion is that the simulation model is set up with source- and sink terms for the transport process of interest. For instance, a thermal gradient is generated with heat source and –sink terms in the form of kinetic energy source and –sink [21] or walls [20]. Alternatively, the heat source and sink may be implemented as thermostatted regions of the system. The thermostats operate typically with a simple velocity scaling algorithm that conserves energy and momentum like in the HEX algorithm [22] or the RNEMD algorithm [24,25]. These methods differ little in principle, and the choice between them is a matter of taste. Like all algorithms operating on single-particle velocities,[1] the source- and sink regions of the system may be considered as separate systems contributing to the transport processes in the bulk of the system like diffuse walls. If it is important to control the system's temperature settings, such as the location in the system's phase diagram, thermostats are preferable. If it is important to control the heat flow or energy conservation, the HEX- or similar algorithms are preferable. The reader should be aware that a defect in the original implementation of the HEX algorithm was corrected recently by Wirnsberger *et*. *al*. [26] in the EHEX algorithm with excellent energy conservation.

[1] Unlike for example dissipative-particle thermostats.

Most simulations aim at reaching a stationary state where mass fluxes have decayed to zero mean values. Although experiments with transient states were made and analysed, few simulations have addressed transient behaviours [27]. In the present paper, we examine transient properties of coupled heat and mass transport in a binary mixture and show that (at least in simulations) it is possible to extract reliable data for the Soret coefficient from the transient states.

This paper addresses the following questions:

(1) A sudden local heating gives a pressure increase ranging from a mild sound wave to an explosion. How does the pressure propagate through the system, and is its effect sufficiently distinct from the Ludwig-Soret effect in space and time to allow for determination of the latter in a transient experiment?

(2) A local heat source gives a temperature gradient. How fast do the components in a mixture separate due to the Ludwig-Soret effect shortly after the heat is turned on?

(3) Is local equilibrium fulfilled, so that the irreversible thermodynamics formalism may be used?

(4) If there is local equilibrium, can the Soret coefficient be determined from data acquired during the transient period?

NEMD simulations allow for detailed analyses of the system's properties and transport processes as functions of space and time. In this work, we have employed BD-NEMD as described by Ikeshoji and Hafskjold [21]. The results from the simulations are interpreted in terms of the formalism given by irreversible thermodynamics [4] as described in Section 2. The details of the simulations are given in Section 3 and the results are presented in Section 4. In order to connect the NEMD results to irreversible thermodynamics, the assumption of local equilibrium in the system was analysed as described in Section 5. The conclusion from this analysis was then used to discuss the time-dependent Soret coefficient as described in Section 6.

2. Theory

In a binary mixture of non-ionic molecules subject to a temperature gradient, there are two diffusive transport processes, a heat flux and a mass flux. We consider here a three-dimensional system with fluxes and forces in one direction only (the x-direction). The transport equations may be expressed as

$$J_q = -L_{qq}\frac{\nabla T}{T^2} - L_{q1}\frac{1}{T}\nabla_T(\mu_1 - \mu_2) \tag{1a}$$

$$J_1 = -L_{1q}\frac{\nabla T}{T^2} - L_{11}\frac{1}{T}\nabla_T(\mu_1 - \mu_2) \tag{1b}$$

where J_q is the heat flux[2], J_1 the mass flux of component 1 (the other mass flux depends trivially on J_1 through the reference frame), the coefficients L are the phenomenological transport coefficients, T is the temperature, and μ_k is the chemical potential of component k. The subscript "T" denotes that the gradient in the chemical potential shall be taken at isothermal conditions.

The mass flux in Eq. (1b) may alternatively be expressed in a mean molar reference frame as

$$J_1 = -nx_1x_2D_T\nabla T - nD\nabla x_1 \tag{2}$$

where n is the number density, D_T the thermal diffusion coefficient, D the mutual diffusion coefficient and x_k the mole fraction of component k. The two diffusion coefficients are related to the phenomenological transport coefficients by

$$D_T = \frac{L_{1q}}{nx_1x_2T^2} \tag{3}$$

and

$$D = \frac{L_{11}}{nx_2T}\frac{\partial\mu_1}{\partial x_1} \tag{4}$$

The Soret coefficient is defined as

$$S_T = \frac{D_T}{D} \tag{5}$$

[2] The heat flux is sometimes called the energy flux to distinguish it from the measurable heat flux, see *e.g.* ref. [4].

At stationary state ($J_1 = 0$), the Soret coefficient may be expressed as

$$S_T = -\frac{1}{x_1 x_2}\left(\frac{\nabla x_1}{\nabla T}\right)_{J_1=0} \tag{6}$$

The quantities on the rhs of Eq. (6) are thus function of space (x), but not of time.

Equation (2) is, however, valid also in transient states. The Soret coefficient may in such case be expressed by rearranging Eq. (2):

$$S_T = \frac{D_T}{D} = -\frac{1}{w_1 w_2}\left(\frac{\nabla w_1}{\nabla T}\right) - \frac{J_1}{w_1 w_2 n D \nabla T} \tag{7}$$

This expression may be used to analyse NEMD data as all the quantities are mechanical and functions of space and time, provided local equilibrium is fulfilled. The question that will be addressed in the following sections is whether it is possible or convenient to use Eq. (7) for determining S_T. The first term on the rhs of Eq. (7) is independent of the reference frame for a binary system, and so is the second term as long as J_1 and D are computed in the same reference frame. In the following, we shall use the mean molar reference frame for this term.

Eq. (7) shows that the advantage of a stationary-state method is to avoid the need for data on J_1 and D, which are not easily obtained in a transient experiment. The purpose of this paper is therefore to examine the contribution to S_T from the second term in Eq. (7).

3. NEMD simulations

A binary isotope mixture was modelled with a Lennard-Jones/spline (LJ/s) potential defined by the pair potential [28]

$$u(r) = \begin{cases} 4\varepsilon_{ij}\left[\left(\frac{\sigma_{ij}}{r}\right)^{12} - \left(\frac{\sigma_{ij}}{r}\right)^{6}\right] & \text{for } r \le r_s \\ a_{ij}(r - r_c)^2 + b_{ij}(r - r_c)^3 & \text{for } r_s \le r \le r_c \\ 0 & \text{for } r \ge r_c \end{cases} \tag{8}$$

where

$$r_s = \left(\frac{26}{7}\right)^{1/6} \sigma_{ij} \tag{9a}$$

$$r_c = \frac{67}{48} r_s \tag{9b}$$

$$a_{ij} = -\frac{24192}{3211} \frac{\varepsilon_{ij}}{r_s^2} \tag{9c}$$

and

$$b_{ij} = -\frac{387072}{61009} \frac{\varepsilon_{ij}}{r_s^3} \tag{9d}$$

The parameters ε_{ij} and σ_{ij} are the usual Lennard-Jones parameters. The LJ/s potential was chosen because it is uniquely defined with zero potential energy and zero force at $r = r_c$ and of shorter range than a typical truncated LJ potential (at $r_c = 2.5\sigma$ or larger), while containing essentially the same physics as the LJ potential.

The system was a binary mixture with all molecular diameters being equal and all potential depths being equal, *i.e.* $\sigma_{ij} = \sigma$ and $\varepsilon_{ij} = \varepsilon$ for all combinations of *i* and *j*. The only difference between the components was the mass with a ratio, $\frac{m_2}{m_1} = 10$, *i.e.* an "isotope" mixture. It is known that for this mixture, the heavier component (component 2) migrates to the system's cold region [21].

A BD-NEMD method as described by Ikeshoji and Hafskjold [21] and by Hafskjold *et. al*. [22] was used, except that the HEX algorithm was replaced by thermostats in the boundary layers. A sketch of the NEMD cell layout is shown in Figure 1.

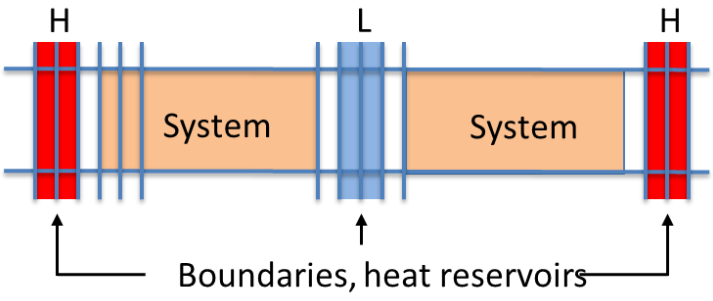

Figure 1. NEMD cell layout. Please see text for explanation.

The cell was non-cubic with an aspect ratio $L_x : L_y = L_x : L_z = 32$ with periodic boundary conditions in all three directions.

The cell was divided into 128 layers of equal thickness perpendicular to the x-direction. One layer at each end was thermostatted to a temperature T_{H} and the two layers in the center of the cell was thermostatted to a temperature T_{L}. The thermostats used a simple velocity rescaling algorithm with local momentum conservation,

$$\mathbf{v}_i^{\mathrm{new}} = \gamma_k \mathbf{v}_i^{\mathrm{old}} + \boldsymbol{\beta} \tag{10}$$

where $\mathbf{v}_i^{\mathrm{old}}$ and $\mathbf{v}_i^{\mathrm{new}}$ are the velocity of particle i before and after the rescaling, respectively. The parameters γ_k and $\boldsymbol{\beta}$ were determined so as to adjust the velocity distribution of particles of each species k to the set kinetic temperature while retaining a local zero total momentum of all the particles in the thermostatted layers. Unless the thermostat was independently applied to the x-, y-, and z-components of the velocities, the temperature in the hot region developed a non-isotropic profile due to heat loss in the x-direction.

The regions marked "System" in the figure, separated from the thermostatted layers by at least one layer, was used for acquiring thermodynamic and transport data. The symmetry of the system was used to pool data from the left and right sides of the cold layers.

The simulations were done with $N = 128{,}000$ particles and overall mole fractions $x_1 = x_2 = 0.5$. The phase diagram of the 3D LJ/s system shows gas, liquid, and solid phases with a critical temperature $T_{\mathrm{c}}^* \approx 0.9$ in reduced Lennard-Jones units, a critical number density $n_c^* \approx 0.4$, and a triple-point temperature $T_{\mathrm{tp}}^* \approx 0.5$. Three cases were studied in this work, at overall densities $n^* = 0.02$, 0.4, and 0.8.

The system was first equilibrated at a uniform temperature $T^* = 2.0$. At time zero, the thermostat set point in the hot layers was suddenly (at time $t^* = 0$) set to $T_{\mathrm{H}}^* = 10.0$ and maintained at that value as shown in Figure 2 while the cold layers were kept at $T_{\mathrm{L}}^* = 2.0$. The system in all the other layers was free to adjust its properties according to the impact from the thermostatted layers. The system's response was monitored from then on.

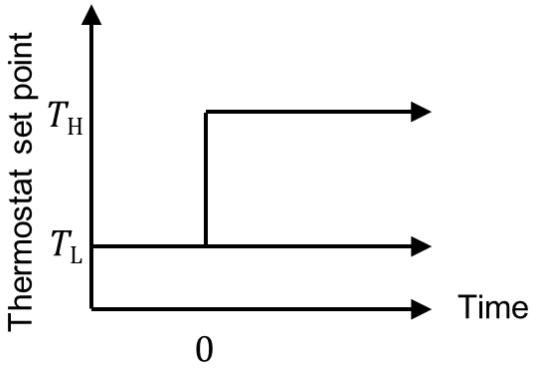

Figure 2. Generation of transient states by suddenly increasing the temperature in the hot layers.

Other values of T_{H}^* and T_{L}^* as well as pulsed heat source were also used without giving significantly different results from those reported here. These results are therefore not included in this paper.

In order to estimate the magnitude of random errors in the transient phase, 20 runs were started from different equilibrium configurations, generated by initial Monte Carlo sequences of different lengths at $T^* = 10.0$, then cooled down to $T^* = 2.0$ and allowed to equilibrate with equilibrium MD. The time step was in all cases $t^* = 0.002$ with the reduced time defined as $t^* = \frac{t}{\sigma}\left(\frac{\varepsilon}{m_1}\right)^{½}$.

Instantaneous values for the properties of interest were acquired for each layer every 20 time step and accumulated for computation of averages over time intervals Δt^* to obtain local properties. The values of Δt^* are given in Table I. For comparison, the mean free path λ^* as computed from elementary kinetic theory is also given in the table.

Table I. Parameters used for computation of local averages in space and time. The mean free path λ^* is included for comparison with the layer thickness Δx^*. In all cases, $T_{\mathrm{H}}^* = 10.0$ and $T_{\mathrm{L}}^* = 2.0$.

Case	n_{overall}^*	Δx^*	$L_x^*/2$	λ^*	Δt^*	t_{run}^*
Liquid	0.8	4.28	272.6	0.28	0.4	160
Supercritical	0.4	5.39	343.3	0.56	0.8	200
Dense gas	0.02	14.62	931.2	11.25	2.0	600

The local kinetic temperature was computed as

$$T = \frac{1}{3Nk_B} \sum_{i \epsilon \mathrm{CV}} m_i (\mathbf{v}_i - \mathbf{v}_{\mathrm{cm}})^2 \tag{11}$$

Here, $\mathbf{v}_i$ is the instantaneous velocity of particle i and k_B is Boltzmann's constant. The centre-of-mass velocity $\mathbf{v}_{\mathrm{cm}}$ was averaged over the local control volume (layer) $\mathrm{CV}^* = \Delta x^* L_y^* L_z^*$, where Δx^* is the thickness of each layer as listed in Table I, and the interval Δt^*.

The local mass flux of component k was computed as

$$J_k = \frac{1}{V} \sum_{i \epsilon \mathrm{CV}} m_i (\mathbf{v}_i - \mathbf{v}_{\mathrm{mm}}) \tag{12}$$

where $\mathbf{v}_{\mathrm{mm}}$ is the mean molar velocity.

The consequence of the time averaging over Δt^* was that the shock wave that passed by the observation "window" at a given position (a given value of x^*) was smoothed. In particular, the shock front appears less steep than the instantaneous value.

4. Results

The sudden increase in the hot-layer temperature generated a pressure wave in the system. As an example, Figure 3 shows the pressure profile in the supercritical mixture shortly after the heat is turned on, at $t^* = 52$. The pressure wave travels faster than the speed of sound and resembles a shock wave through the system except that the front is smoothed as described in Section 3. Due to the symmetry of the system, a mirror of the wave travels from the other end of the MD cell. The two waves meet, are reflected, and travel back and forth until they eventually die out, giving a stationary state with uniform pressure. The length of each production run was chosen so that the shock wave just reached the centre of the MD cell.

The temperature profile shown in Figure 4 also shows a shock wave behaviour in addition to the expected diffusion of heat near the hot layer. The shock wave behaviour and the heat diffusion will be further analysed in a forthcoming paper, but the conclusion is that the thermal diffusivity of the

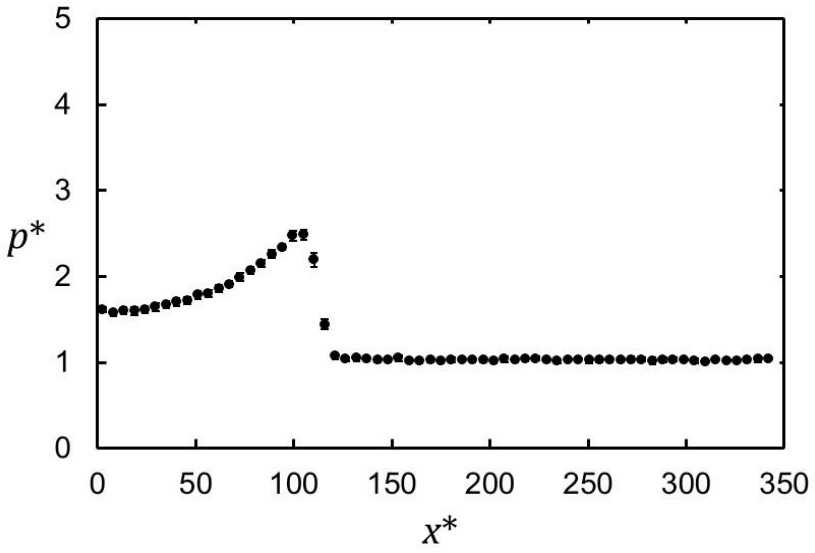

Figure 3. Pressure profile in the binary isotope mixture at overall number density $n^* = 0.4$ and at time $t^* = 52$ after the heat is turned on with $T_H^* = 10$ while T_L^* is kept at $T_L^* = 2$. The distance from the hot end of the MD cell is x^* (in LJ units). The uncertainties, reported as three standard deviations of the mean, are smaller than the symbol size, except in the shock front.

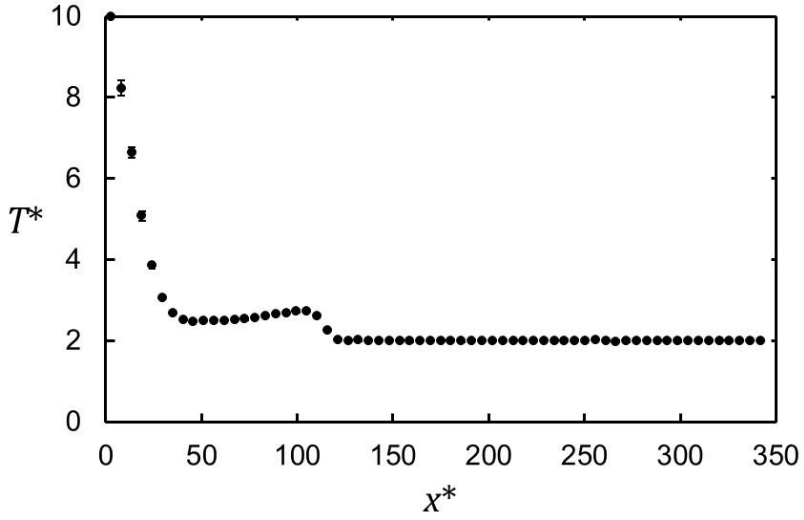

Figure 4. Temperature profile at the same condition as shown in Figure 3.

mixture may be determined from the temporal evolution of the temperature profile near the hot layer.

Here, we shall analyse how the composition profile develops in the transient phase. The mole fraction of (the lighter) component 1 at the same condition and time as for the shown pressure and temperature profiles is shown in Figure 5. In the bulk of the system, the equilibrium composition $x_1 = 0.5$ is retained at this time, $t^* = 52$. Near the heat source, the two components have to some extent

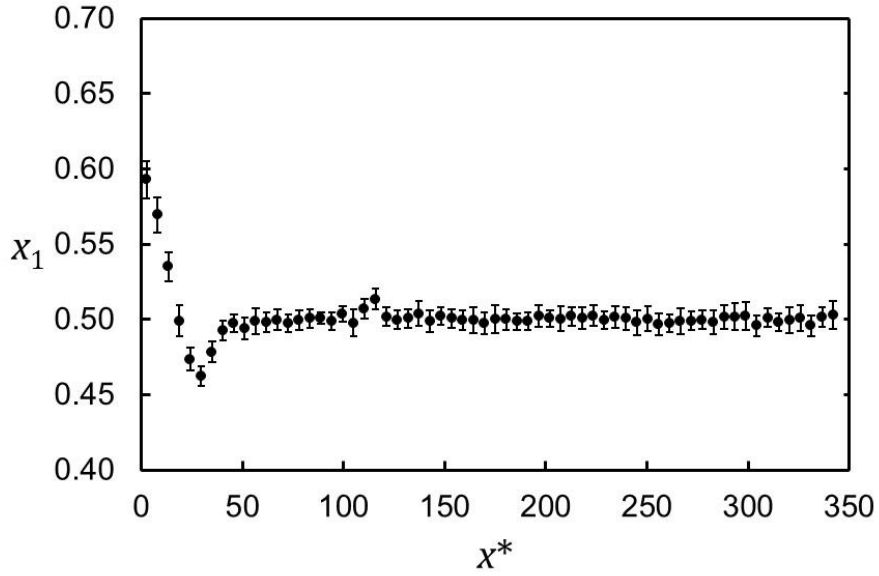

Figure 5. Mole fraction of component 1 as function of distance from the hot layer at the same condition as shown in Figure 3. A distinct composition profile has developed for $0 < x^* \lesssim 30$. There is also a small peak in the composition profile at $x^* \sim 110$, the position of the shock wave at this time.

separated as shown by the distinct profile in the range $0 < x^* \lesssim 30$. This behaviour is accentuated at later times, but within the time frame of this simulation it is restricted to the region near the heat source. Eventually, the composition will show a more linear profile over the whole range of x^* when the system has reached stationary state.

One might think that acceleration of the lighter component 1 due to the sudden temperature increase would deplete this component in the region near the heat source. The results show that the opposite happens, the heavier component is depleted in the hot region. This means that the Soret effect is dominant immediately after the heat is turned on.

Similar results were obtained for the liquid and dense gas states.

Figures 3 – 5 show the expected behaviour that (1) the pressure wave travels fast and the pressure becomes quite uniform in the wake of the shock, (2) the heat diffuses out from the heat source, presumably at a rate governed essentially by the thermal diffusivity of the system, and (3) the overall composition profile develops slowly. The small peak in the mole fraction near the position of the shock wave will not be further analysed here as the statistics do not allow for conclusive results at this time.

One way to present the relation between mole fraction and temperature profiles is to consider the ratio between the gradients, inspired by Eq. (7). The ratio between the gradients may be expressed as

$$\frac{\nabla x_1}{\nabla T} = \left(\frac{\partial x_1}{\partial T}\right)_{t^*} \tag{13}$$

so by plotting x_1 as function of T^*, we can determine the first term on the rhs of Eq. (7). The plot is shown for selected times in Figure 6. These data were obtained from the layers close to the hot layer, in the region where the mole-fraction in Figure 5 shows a distinct declining profile. The point at the highest temperature for each time represents the hot layer. This point and the one at the second highest temperature were not included in the analysis to avoid possible artefacts of the thermostat. The temperature and mole fraction in the following three layers down the temperature profile (the encircled points in Figure 6) were then used to estimate the ratio needed to compute the Soret coefficient from Eq. (7).

In the transient phase, we also need the mass flux and the mass diffusion coefficient to complete the analysis based on Eq. (7). The mass flux was readily obtained in the NEMD simulation from Eq. (12). An example is shown in Figure 7, representing the same condition and time as shown in Figures 3 – 5.

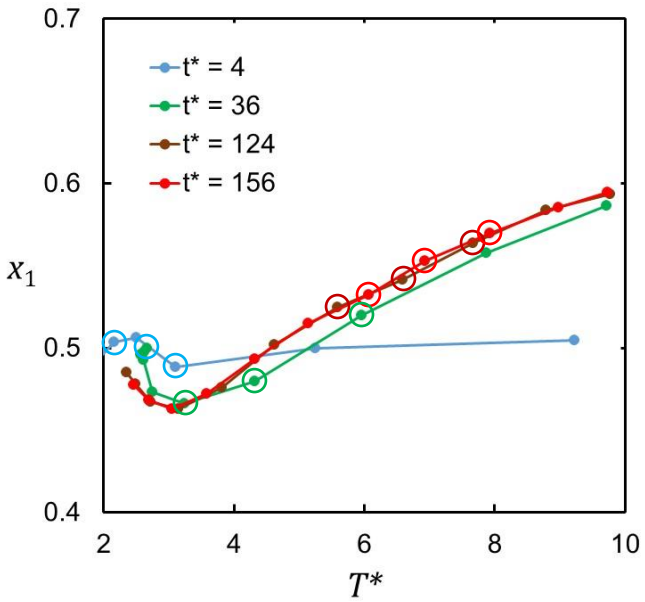

Figure 6. Local mole fraction of component 1 as function of local temperature near the hot layer. The data points used to compute the gradients (Eq. (16)) are encircled (see text).

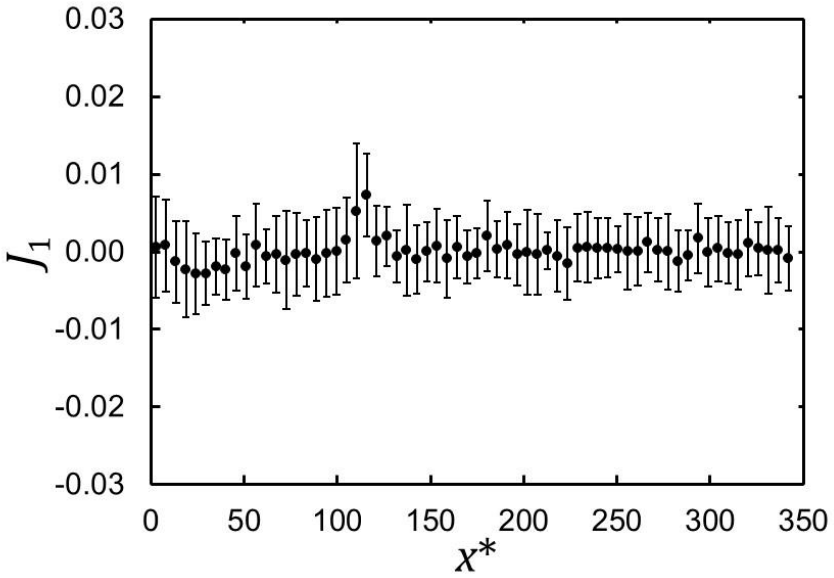

Figure 7. Mean molar mass flux at the same condition as shown in Figure 3.

At this time, there is still a small negative mass flux near the heat source, although not significantly different from zero. The mass flux has essentially vanished at this time. The diffusion constant was determined from two independent NEMD simulations with the MEX algorithm [29]. The MEX algorithm generates a concentration gradient in the binary system by imposing a mass flux and is in practice similar to the HEX algorithm. The ratio between the mass flux and the concentration gradient enables a determination of the product nD that is needed in Eq. (7). Two simulations were made with 4000 particles with independent and local thermostatting to a fixed temperature in all layers to ensure isothermal conditions. The density and temperature in the two cases were chosen so as to represent the regions used for analysis (the encircled points in Figure 6). It turned out that the product of density and mutual diffusion coefficient was quite independent of the conditions; for the state points $(T^* = 6.4, n^* = 0.204)$ and $(T^* = 7.0, n^* = 0.350)$, the values were $n^*D^* = 0.399$ and 0.378, respectively. Moreover, J_1 quickly fluctuated around zero mean value, so that an uncertainty in the product n^*D^* was found to have little effect on the determination of S_T.

5. A note on local equilibrium and the use of linear irreversible thermodynamics.

Eq. (7) is based on the formalism of linear irreversible thermodynamics, which assumes local equilibrium in the system. Before proceeding with the analysis of the data in terms of Eq. (7), we

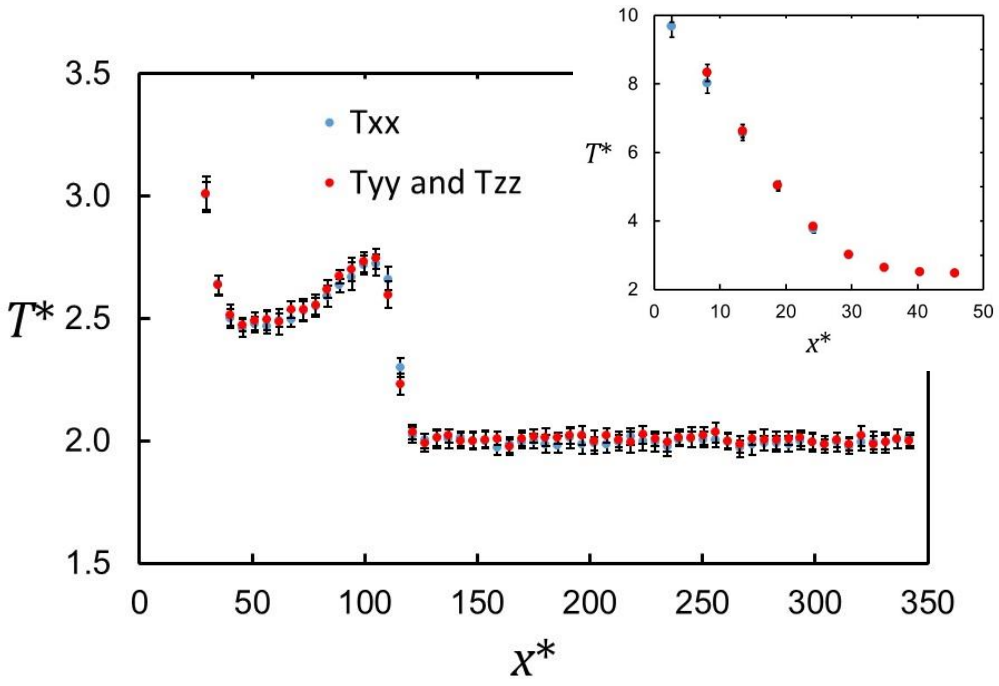

Figure 8. Comparison between the three diagonal components of the pressure tensor. All three components are equal to within combined random errors, except in the shock front.

must therefore determine whether or not the system in fact fulfils local equilibrium in the transient phase. Based on our previous work [29], we have chosen to consider two indicators: (1) isotropy of the kinetic temperature and (2) the values of local thermodynamic properties in relation to the equilibrium equation-of-state values. The idea is that if one or both of these conditions are violated,local equilibrium is not fulfilled. The opposite case is a strong indication that local equilibrium is fulfilled.

The kinetic temperature determined by Eq. (11) is a tensor. If the components of the tensor are equal, the temperature may be considered to be isotropic. Figure 8 shows that the diagonal elements T_{xx}, T_{yy}, and T_{zz}, are equal to within combined errors, except in the shock front. In the present context, the region near the hot source is of greatest interest. In this region, there is no indication that the local-equilibrium assumption is violated.

The components of the pressure tensor show a similarly good agreement (not included here). The case shown in Figure 8 is for the same state as shown in Figure 4, *i.e.* overall density approximately critical ($n^* \approx 0.4$). The same isotropic behavior was also found in the liquid case, whereas in the dense

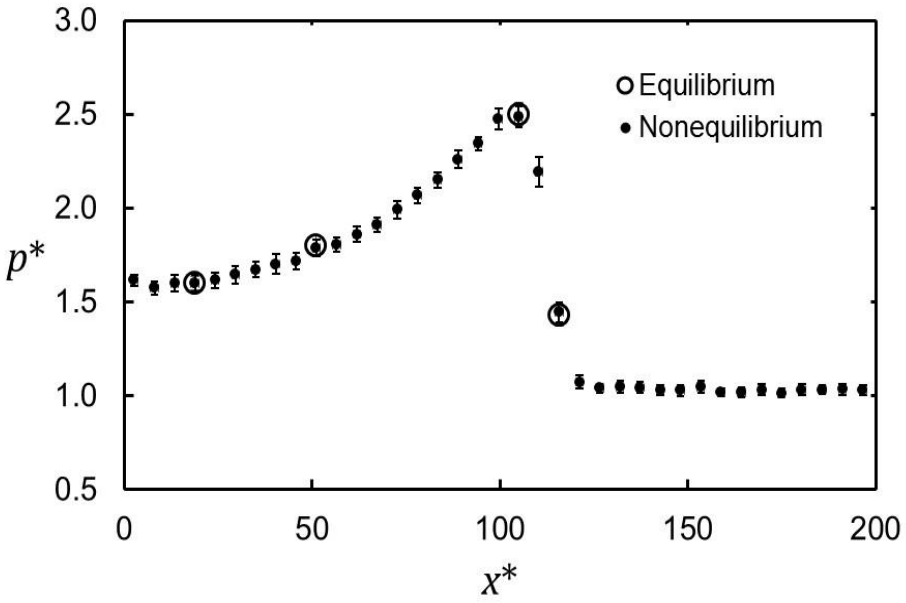

Figure 9. Comparison between the local pressure from a nonequilibrium simulations transient at $t^* = 52$ and four equilibrium values at the densites and temperatures taken from the nonequilibrium results. The four nonequilibrium states used for comparison are specified in Table II.

gas case, $n^* \approx 0.02$, the T_{xx} was slightly more different from T_{yy} and T_{zz} than in the supercritical case in the region of the shock front.

The other check on local equilibrium was based on comparing the local equation of state in the transient case with results from equilibrium simulations. Four state point were chosen from the non-equilibrium simulation. As an example, the supercritical case at $t^* = 52$ is included here. Equilibrium NVT-simulations were done with $N = 4000$ and the selected densities and temperatures as input, and the corresponding pressure and enthalpy were computed. The comparison is shown in Figure 9 for the pressure and Figure 10 for the enthalpy. These comparisons also show that the local equilibrium condition is not violated. Equally close similarity between non-equilibrium and equilibrium results were found also in the liquid and dense gas cases, see Table II for comparison of the pressures.

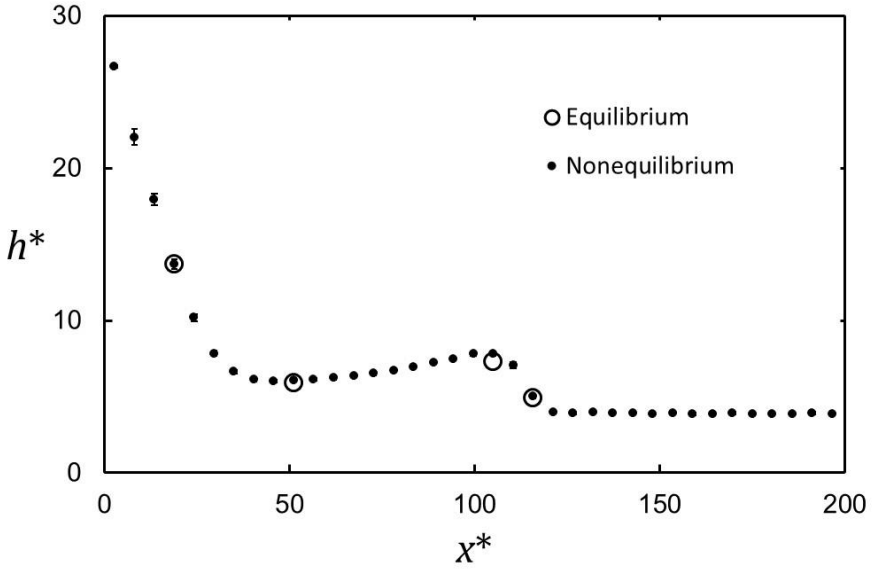

Figure 10. Comparison between the nonequilibrium and equilibrium enthalpy per particle. Otherwise the same case as shown in Figure 9.

Table II. Comparison between local pressures from the non-equilibrium simulation with equilibrium values at the same temperature and number density. The mole-fraction values are included, but have no importance for the thermodynamic properties of this isotope mixture. Note that the dense gas is close to ideal, $p^* = n^* T^*$.

Case	x^*	T^*	n^*	x_1^*	p^*_{NEMD}	p^*_{eq}
Liquid	15.0	3.44	0.710	0.46	8.03 ± 0.15	8.08 ± 0.04
	49.2	2.24	0.829	0.50	8.70 ± 0.12	8.72 ± 0.05
	100	2.52	0.883	0.50	12.5 ± 0.2	12.58 ± 0.06
	113	2.17	0.829	0.51	8.5 ± 0.2	8.43 ± 0.04
Supercritical	18.9	5.08	0.238	0.50	1.60 ± 0.05	1.605 ± 0.008
	51.2	2.48	0.452	0.49	1.74 ± 0.04	1.80 ± 0.01
	105	2.74	0.497	0.50	2.49 ± 0.06	2.50 ± 0.01
	143	2.25	0.432	0.51	1.45 ± 0.03	1.43 ± 0.01
Dense gas	51.2	7.52	0.0087	0.52	0.066 ± 0.002	0.0662 ± 0.0006
	212	3.74	0.0177	0.48	0.067 ± 0.001	0.0671 ± 0.0005
	344	2.70	0.0269	0.49	0.073 ± 0.001	0.0735 ± 0.0006
	402	2.66	0.0283	0.50	0.076 ± 0.001	0.0761 ± 0.0006
	519	2.38	0.0239	0.52	0.057 ± 0.001	0.0572 ± 0.0005

The conclusion is a strong indication that local equilibrium is fulfilled and that the data may be analysed in terms of the formalism of irreversible thermodynamics.

We can now complete the analysis in terms of Eq. (7). The two terms on the rhs of Eq. (7) and their sum were computed as function of time as described above for the liquid, supercritical, and dense gas states. The results are shown in Figure 11. The data show that the second term in Eq. (7) decays quickly to zero and that the first term then gives the steady-state value for the Soret coefficient.

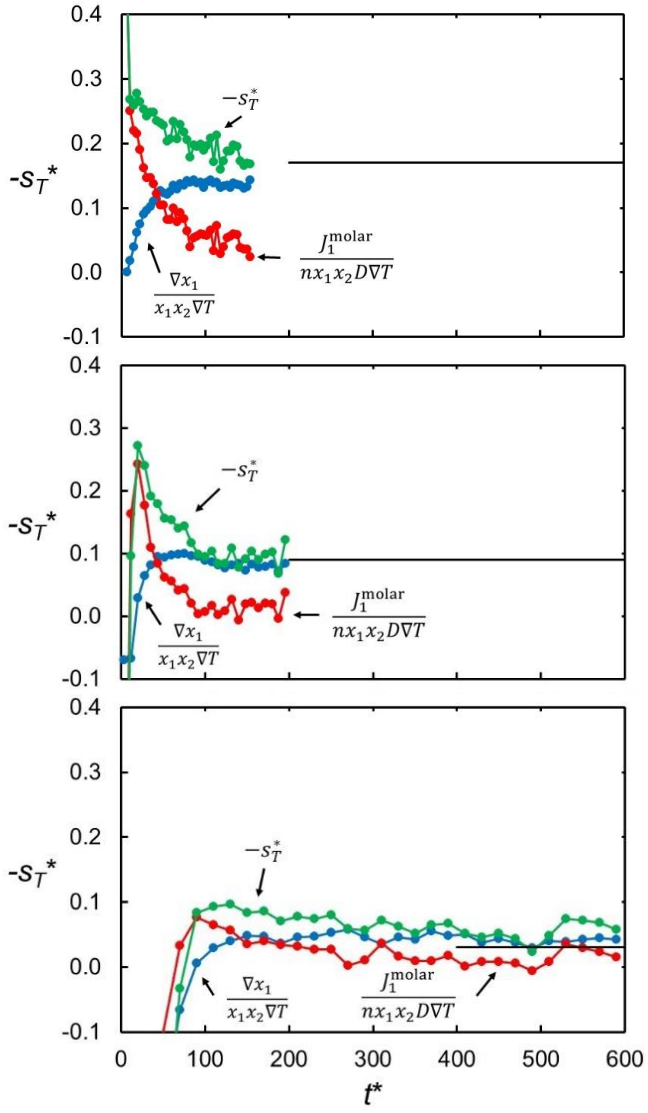

Figure 11. Development of the Soret coefficient and its two contributions with time (Eq. (6)). The three diagrams show a liquid state (top), supercritical state (middle), and dense gas (bottom). The states are specified in Table I. The horizontal black line represent stationary state values obtained from independent, NEMD simulations with N=4000 particles. Please note that the sign of S_T is just a chosen way to represent that data since component 2 is the heavier component in this work.

6. Discussion

In a recent paper, Ferrario et al. [27] studied the onset of a temperature-, density-, and composition gradient in a binary Lennard-Jones mixture representing Ar and Kr at equimolar composition. They used the D-NEMD method [30] and computed the Soret coefficient when the system had reached a stationary state. The present paper is similar in the sense that the initial phase of the system's response to a thermal perturbation is studied, but we focus on the transient phase and show that it is possible to use such data to determine the Soret coefficient, thus avoiding the need for stationary state. Although analyses of transient experimental data have been made, we are not aware of any other NEMD simulation in which the Soret effect has been analysed in this way.

The complete data sets of $T(x,t)$, $x_1(x,t)$, and $J_1(x,t)$ contain in principle information about the diffusion coefficient and the Soret coefficient. A complete analysis would require a theoretical framework for the time evolution of S_T along the lines shown by Van Vaerenbergh and Legros [31], Costesèque *et. al.* [32], and Mialdun and Shevtsova [17]

The analysis shown here is based on measuring the composition and temperature as function of distance from the heat source for fixed time. In an experimental setup, it may be more convenient to measure the composition as function of time for a fixed distance from the heat source. The NEMD simulation provides data as function of both space and time and the question is how such data can be used in analysis of experimental data. Figure 12 shows the time evolution of T^* and x_1 for three fixed distances from the heat source. The distances were selected in the region where the concentration gradient developed, which requires some prior knowledge about the evolution of the Soret coefficient. If we approximate

$$\frac{\nabla x_1}{\nabla T} \approx \left(\frac{\Delta x_1}{\Delta T}\right)_{t^*} \tag{16}$$

where "Δ" denotes a difference between two of the curves in Figure 12 indicated by the arrows, and plot $\frac{\Delta x_1}{x_1 x_2 \Delta T}$ as function of time, we get graphs like the two shown in Figure 13.

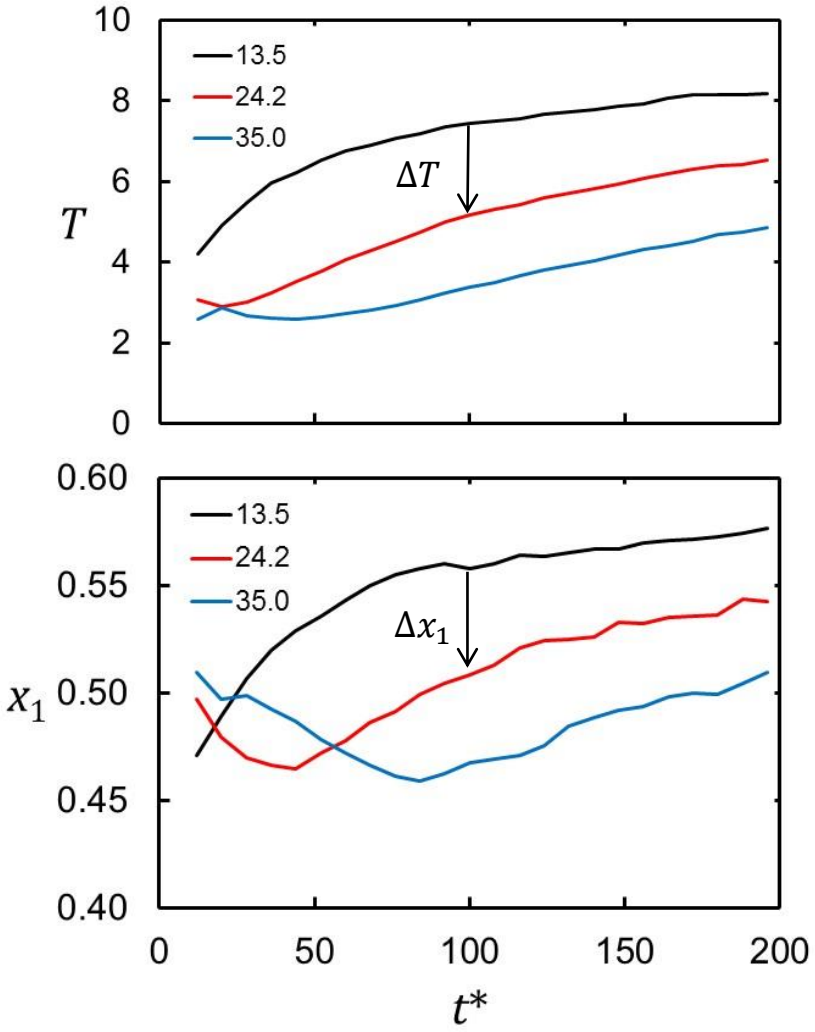

Figure 12. Temperature (top) and mole fraction of component 1 (bottom) as function of time for three different distances from the hot layer, $x^* = 13.5, 24.2$, and 35.0, for the supercritical state. The arrows indicate differences in T and x_1 that may be used to determine the Soret coefficient (see text).

Compared with the results shown in Figure 11, this rough method gives a pretty good estimate for the Soret coefficient. The three choices for the distance from the heat source give different results for the shortest times, but they quickly converge to the stationary-state value. The results appear not to be very sensitive to how the distances from the heat source are selected as long as they are in the region where the concentration gradient is quickly established.

If it is not possible to distinguish between the effects of temperature and composition in a measurement, a possible route to the temperature profile may be to solve the transient heat equation. This will, however, not be further discussed here, but it would be interesting to compare

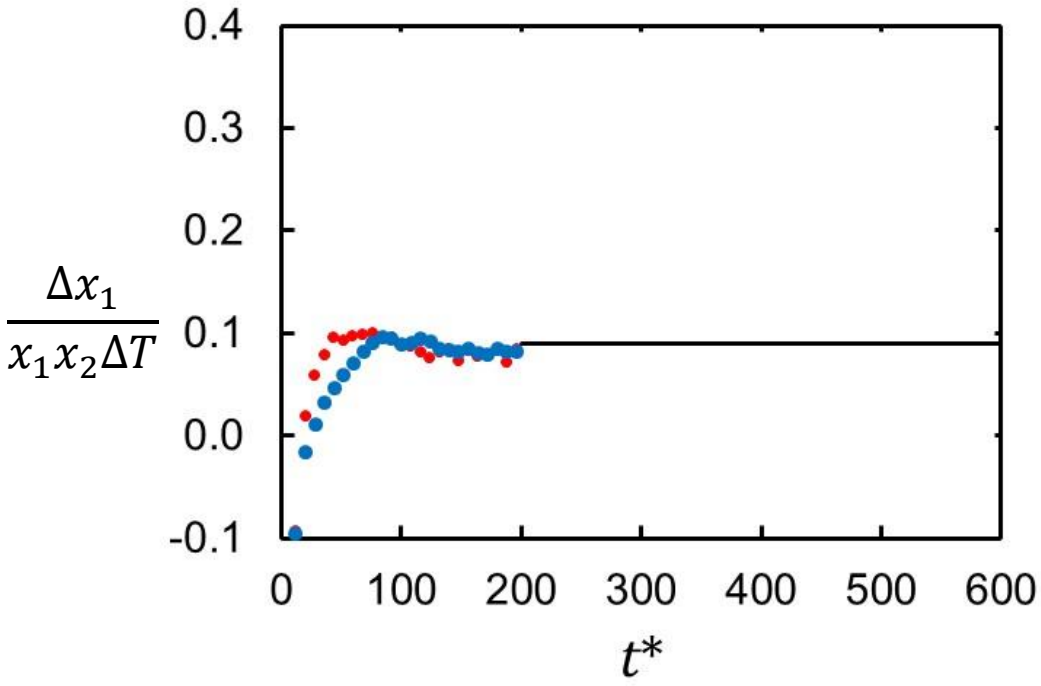

Figure 13. Estimates of the Soret coefficient. The blue dots are based on the difference between the blue and the black curves in Figure 12 and the red dots are from the difference between the red and the black curves. The black line is the result from a stationary-state simulation as described in Section 5.

results from simulations and experiments designed for transient measurements of both D_T and D [32-34].

7. Conclusions

The main conclusion from the present work is that the Soret effect in a binary fluid mixture may be observed immediately after the heat has been switched on and in the vicinity of the hot layer. The local temperature gradient immediately gives a local component separation, whereas separation in the bulk is slow. Local equilibrium is fulfilled in the cases studied here. Assuming local equilibrium, the Soret coefficient can be determined during the transient period. Using the transient is not an efficient way to compute the Soret coefficient, but may give a useful route to experimental techniques in the presence of gravity.

Acknowledgements

This work started as a project with students Sandra Sæther and Jacob Hadler-Jacobsen, with whom I had interseting discussion during problem formulation. Good introductory discussions with Fernando Bresme, Miguel Rubi, Dick Bedeaux, Signe Kjelstrup, and Magnus Heskestad Waage were also highly appreciated. Comuter resources have been provided by Faculty of Natural Sciences and Technology at NTNU and by the HPC resources at UiT provided by NOTUR, http://www.sigma2.no.

References

[1] Ludwig, C. (1856), "Diffusion zwischen ungleich erwwärmten orten gleich zusammengestzter lösungen," Sitz. Ber. Akad. Wiss. Wien Math-Naturw. Kl., **20**, 539.

[2] Soret, Ch. (1879) "Sur l'état d'équilibre que prend au point de vue de sa concentration une dissolution saline primitivement homohéne dont deux parties sont portées à des températures différentes," Arch. Sci. Phys. Nat., **2**, 48–61.

[3] deGroot, S. and Mazur, P. (1984), "Non-equilibrium Thermodynamics", Dover.

[4] Kjelstrup, S., Bedeaux, D., Johannesen, E., and Gross, J. (2010), «Non-Equilibrium Thermodynamics for Engingeers», World Scientific, New Jersey.

[5] Bou-Ali, M.M. *et*. *al*. (2015), "Benchmark values for the Soret, thermodiffusion and molecular diffusion coefficients of the ternary mixture tetralin+isobutylbenzene+n-dodecane with 0.8-0.1-0.1 mass fraction", Eur. Phys. J. E, **38**, 15030-7.

[6] Artola, P.-A. and Rousseau, B. (2013) "Thermal diffusion in simple liquid mixtures: what have we learnt from molecular dynamics simulations?", Mol. Phys., **111**, 3394-3403.

[7] Firoozabadi, A, Ghoryaeb, K, and Shukla, K (2000), "Theoretical Model of Thermal Diffusion Factors in Multicomponent Mixtures", AIChE Journal **46**, 892-900.

[8] Bordat, P., Reith, D., and Müller-Plathe, F. (2001), "The influence of interaction details on the thermal diffusion in binary Lennard-Jones liquids", J. Chem. Phys. *115*, 8978-8982.

[9] Galliero G. *et*. *al*. (2003), "Thermal diffusion sensitivity to the molecular parameters of a binary equimolar mixture, a non-equilibrium molecular dynamics approach", Fluid Phase Equil. **208**, 171-188.

[10] Köhler, W. and Morozow, K.I. (2016) "The Soret Effect in Liquid Mixtures - A Review", J. Non-equilibrium Thermodynamics, **41**, 151-197.

[11] Srinivasan, S. and Saghir, M.Z. (2011) "Experimental approaches to study Thermodiffusion – A review", Int. J. Therm. Sci., **50**, 1125-1137.

[12] Platten, J.K. (2006), "The Soret Effect: A Review of Recent Experimental Results", J. Appl. Mech., **73**, 5-15.

[13] Wiegand, S. (2004), "Thermal diffusion in liquid mixtures of polymer solutions", J. Phys.: Condens. Matter, **16**, R357-R379.

[14] Putnam, S.A. and Cahill, D.G. (2004), "Micron-scale apparatus for measurements of Thermodiffusion in liquid", Rev. Sci. Instruments. **75**, 2368-2372.

[15] Pohl, D.W, Schwarz, P., and Irniger, V. (1973), "Forced Rayleigh Scattering", Phys. Rev. Lett. **31**, 32-35.

[16] Thyagarajan, K. and Lallemand, P. (1978), "Determination of the thermal diffusion ratio in a binary mixture by forced Rayleigh scattering", Optics Comm. **26**, 54-57.

[17] Mialdun, A. and Shevtsova, V. (2011), "Measurement of the Soret and diffusion coefficients for benchmark binary mixtures by means of digital interferometry", J. Chem. Phys. **134**, 044524-1-12.

[18] MacGowan, D. and Evans, D.J. (1986), "Heat and matter transport in binary liquid mixtures", Phys. Rev. A **34**, 2133-2142.

[19] Paolini, G.V. and Ciccotti, G. (1987), "Cross thermotransport in liquid mixtures by nonequilibrium molecular dynamics", Phys. Rev. A **35**, 5156-5166.

[20] Ashurst, W.T. and Hoover, W.G. (1975), "Dense-fluid shear viscosity via nonequilibrium molecular dynamics", Phys. Rev. A **11**, 658-678.

[21] Ikeshoji, T. and Hafskjold, B. (1994), "Non-equilibrium molecular dynamics calculation of heat conduction in liquid and through liquid-gas interface", Mol. Phys. 81, 251-261.

[22] Hafskjold, B., Ikeshoji, T, and Ratkje, S.K. (1993), “On the molecular mechanism on thermal diffusion in liquids”, Mol. Phys. 80, 1389-1412.

[23] Bresme, F., Lervik, A., and Armstraong, J (2016), “Non-equilibrium Molecular Dynamics», in Experimental Thermodynamics Volume X: Non-equilibrium Thermodynamics with Applications, ed. by Bedeaux, D., Kjelstrup, S., and Sengers, J.V. The Royal Society of Chemistry, Cambridge.

[24] Müller-Plathe, F. (1997), “A simple nonequilibrium molecular dynamics method for calculating the thermal conductivity”, J. Chem. Phys. **106**, 6082-6085.

[25] Reith, D. and Müller-Plathe, F. (2000), “On the nature of thermal diffusion in binary Lennard-Jones liquids”, J. Chem. Phys. **112**, 2436-2443.

[26] Wirnsberger, P. *et*. *al*. (2015), “An enhanced version of the heat exchange algorithm with excellent energy conservation properties”, J. Chem. Phys. **143**, 124104.

[27] Ferrario, M., Bonella, S., and Ciccotti, G. (2016), “On the establishment of thermal diffusion in binary Lennard-Jones liquids”, Eur. Phys. J. Special Topics 1-14.

[28] Holian, B.L. and Evans, D.J. (1983), “Shear viscosities away from the melting line: A comparison of equilibrium and nonequilibrium molecular dynamics”, J. Chem. Phys. **78**, 5147-5150.

[29] Hafskjold, B. and Ratkje, S.K. (1995), “Criteria for Local Equilibrium in a System with Transport of Heat and Mass”, J. Stat. Phys. **78**, 463-494.

[30] Ciccotti, G. and Jacucci, G. (1975), “Direct Computation of Dynamical Response by Molecular Dynamics: The Mobility of a Charged Lennard-Jones Particle“, Phys. Rev. Lett. 35, 789-792.

[31] Van Vaerenbergh, S. and Legros, J.C. (1990), “Kinetics of the Soret effect: Transient in the transport process”, Phys. Rev. A **41**, 6727-6731.

[32] Costesèque, P., Pollak, T., Platten, J.K., and Marcoux, M. (2004), “Transient-state method for coupled evaluation of Soret and Fick coefficients, and related tortuosity factors, using free and porous packed thermodifiusion cells: Application to $CuSO_4$ aqueous solution (0:25 M)”, Eur. Phys. J. E **15**, 249-253.

[33] Haugen, K.B. and Firoozabadi, A. (2007), “Transient separation of multicomponent liquid mixtures in thermogravitational columns”, J. Chem. Phys. **127**, 154507 1-9.

[34] Galand, Q. and Van Vaerenbergh, S. (2015), “Contribution to the benchmark for ternary mixtures: Measurement of diffusion and Soret coefficients of ternary system tetrahydronaphtalene–isobutylbenzene–n-dodecane with mass fractions 80-10-10 at 25 ˚C”, Eur. Phys. J. E **38**: 26 1-10.